Airborne lidar measurements of aerosol optical properties during SAFARI-2000

Matthew J. McGill
Laboratory for Atmospheres, Code 912, NASA Goddard Space Flight Center, Greenbelt, Maryland, USA

Dennis L. Hlavka and William D. Hart
Science Systems and Applications, Inc., NASA Goddard Space Flight Center, Greenbelt, Maryland, USA

Ellsworth J. Welton
Goddard Earth Sciences and Technology Center, NASA Goddard Space Flight Center, Greenbelt, Maryland, USA

James R. Campbell
Science Systems and Applications, Inc., NASA Goddard Space Flight Center, Greenbelt, Maryland, USA

Received 25 March 2002; revised 23 July 2002; accepted 5 August 2002; published 3 April 2003.

[1] The Cloud Physics Lidar (CPL) operated onboard the NASA ER-2 high-altitude aircraft during the Southern African Regional Science Initiative (SAFARI)-2000 field campaign. The CPL provided high spatial resolution estimates of aerosol optical properties at both 1064 and 532 nm. We present here results of planetary boundary layer (PBL) aerosol optical depth analysis and profiles of aerosol extinction. Variation of optical depth and extinction are examined as a function of regional location. The wide-scale aerosol mapping obtained by the CPL is a unique data set that will aid in future studies of aerosol transport. Comparisons between the airborne CPL and ground-based Micro-Pulse Lidar Network (MPL-Net) sites are shown to have good agreement. *INDEX TERMS:* 0305 Atmospheric Composition and Structure: Aerosols and particles (0345, 4801); 3307 Meteorology and Atmospheric Dynamics: Boundary layer processes; 3360 Meteorology and Atmospheric Dynamics: Remote sensing; *KEYWORDS:* lidar, aerosols, SAFARI, optical depth, aerosol extinction

Citation: McGill, M. J., D. L. Hlavka, W. D. Hart, E. J. Welton, and J. R. Campbell, Airborne lidar measurements of aerosol optical properties during SAFARI-2000, *J. Geophys. Res.*, *108*(D13), 8493, doi:10.1029/2002JD002370, 2003.

1. Introduction

[2] The Southern African Regional Science Initiative (SAFARI) during August–September 2000 provided a unique opportunity to study the climatology of southern Africa [*Swap et al.*, 1998, 2002a, 2002b]. Particular emphasis was placed on measurements of biomass burning and regional emissions. Measurement capabilities included ground-based, airborne, and spaceborne instrumentation from active, passive, and in situ sensors. Data from the multiple platforms and sensors will be used to better understand linkages between the land-atmosphere processes that are unique to southern Africa [*Swap et al.*, 2002a, 2002b].

[3] During the SAFARI campaign a high priority was placed on airborne remote sensing measurements using the NASA ER-2 high-altitude aircraft [*King et al.*, 2003]. The SAFARI field campaign was the first field deployment for the new ER-2 Cloud Physics Lidar (CPL). The CPL provided information on cloud height and structure as well as aerosol and smoke plume structure, and aerosol optical depth. Lidar profiling from the ER-2 nearly mimics spaceborne measurements, and the spatial coverage attainable by the ER-2 permits studies of aerosol properties across wide regions of the southern African continent. The large-scale aerosol mapping provided by the CPL will enhance studies of aerosol transport.

[4] The CPL is designed to operate simultaneously at 3 wavelengths: 1064, 532, and 355 nm. However, for the SAFARI campaign the 355 nm channel was not yet operational. Vertical resolution of the CPL measurements is fixed at 30 m. The CPL laser repetition rate is 5 kHz, but profiles are integrated and saved at 10 Hz. Horizontal resolution is therefore 1/10 s (~20 m at typical ER-2 speed of 200 m/s) for raw data, but data are averaged to 1 s for the final data products. The CPL fundamentally measures range-resolved profiles of volume 180-degree backscatter coefficients. From the fundamental measurement, various data products are produced, including: time-height cross-section images; cloud and aerosol layer boundaries; optical depth for clouds, aerosol layers, and planetary boundary layer (PBL); and extinction profiles. All data products are produced for both 532 and 1064 nm. A detailed description of the CPL instrument is beyond the scope of this paper, but details can be found in the work of *McGill et al.* [2002].

0148-0227/03/2002JD002370

[5] During the SAFARI campaign 19 ER-2 flights were conducted, totaling nearly 120 flight hours. In this paper we present selected results from the CPL measurements. A composite of the derived optical depth of the PBL, along with statistics on the optical depth and aerosol extinction form the basis for this work. Comparisons between data from the CPL and ground-based Micro-Pulse Lidars (MPL) in the Micro-Pulse Lidar Network (MPL-Net) [*Welton et al.*, 2001] were made to validate the accuracy of the lidar results. One MPL was located at Skukuza in Kruger National Park in South Africa, the other in Mongu, Zambia. MPL-Net sites are colocated with Aerosol Robotic Network (AERONET) Sun photometers, and each site provides aerosol and cloud layer heights, and estimated profiles of extinction and optical depth for each layer. *Campbell et al.* [2003] discuss the MPL-Net results from SAFARI in more detail.

2. CPL Aerosol Optical Properties Analysis

[6] To obtain cloud or aerosol optical depth from airborne backscatter lidar data requires two primary assumptions regarding the scattering characteristics of the particulates. The first assumption is that multiple scattering can be reliably quantified or neglected. For the CPL instrument multiple scattering is small due to the narrow field of view of the receiver (100 μradians, full angle) and is ignored. The amount of multiple-scattered signal detected depends primarily upon the receiver footprint at the scattering altitude [*Hutt et al.*, 1994]. For a cloud located 10 km from the CPL, the receiver footprint will be only ~1 meter diameter, which is considerably less than the mean free path in optically thin clouds. As described by *Hutt et al.* [1994], contribution of higher-order scattering is minimized as the receiver footprint becomes less than the mean free path.

[7] The second assumption is that the value of the extinction-to-backscatter ratio, or S-ratio, is known. The S-ratio is the total scattered and absorbed energy divided by the amount of backscattered energy. In lidar inversion techniques the S-ratio is generally assumed to be constant throughout a given layer. However, different layers can have dramatically different S-ratios depending on the layer composition. For this reason, it is important that the processing algorithm be able to properly discern aerosol layers and assign to each layer a specific aerosol type (e.g., cloud, elevated aerosol, or PBL). Under certain favorable circumstances, specified below, the S-ratio can be estimated directly from the lidar data without assumption, but more often external information will be required.

[8] The goal of the aerosol optical properties analysis of the CPL lidar signal is to obtain particulate extinction cross-section profiles (σ_P) and particulate layer optical depths (τ_P). The CPL processing scheme first locates the top and bottom of every detectable layer at 1-s resolution and assigns it to be a cloud, elevated aerosol, or PBL. If possible, the transmission loss method (see below) is used to calculate an S-ratio for elevated layers. If the transmission loss method cannot be used, then an S-ratio value is assigned from either an independent measurement or from a look-up table. If an independent measure of the aerosol optical depth is available, such as from a Sun photometer, that value is used to constrain the lidar inversion in estimating the PBL aerosol optical properties in the general vicinity of the Sun photometer site. If no independent estimate is available for the PBL aerosol optical depth, then the CPL processing algorithm defaults to a look-up table of S-values based on regional climatology. The discussion given below restates in part a derivation given many times in the literature [see, e.g., *Spinhirne et al.*, 1980] and only an overview will be provided here.

[9] The working lidar equation for a nadir pointing lidar can be written as:

$$P(z) = \left(\beta_p(z) + \beta_m(z)\right) T_p^2(z) T_m^2(z) \tag{1}$$

where P(z) is the calibrated normalized lidar signal or attenuated backscatter coefficient. The total (particulate and molecular) volumetric backscatter coefficient at distance z is denoted by $\beta(z)$ and the two-way particulate and molecular transmission factor from the aircraft altitude to altitude z is given by $T^2(z)$. The two-way transmission is also expressed as $\exp[-2(\tau_m(z) + \tau_p(z))]$, where τ is optical depth and the subscripts m and p designate molecular and particulate contributions, respectively. Because the molecular contribution to the total backscatter and transmission can be computed from theory, equation (1) is written with the molecular and particulate contributions explicitly separated.

[10] The following relationships relate the two-way transmission to the S-ratio:

$$T_p^2 = e^{-2\int_0^z \sigma_p dz'} \quad \text{and} \quad S_p = \frac{\sigma_p(z)}{\beta_p(z)} \tag{2}$$

and

$$T_m^2 = e^{-2\int_0^z \sigma_m dz'} \quad \text{and} \quad S_m = \frac{\sigma_m(z)}{\beta_m(z)} \tag{3}$$

where S_p and S_m are the particulate and molecular extinction-to-backscatter ratios, respectively, and S_P is assumed constant for each layer. Rayleigh scattering theory can be used to calculate $T_m^2(z)$ if the vertical molecular density profile is accurately known (e.g., provided by sounding data) or can be calculated based on standard atmospheres. The molecular extinction-to-backscatter ratio, S_m is a constant $8\pi/3$ sr. The purpose of the CPL data processing is to solve for the vertical profiles of β_p. The particulate optical depth and extinction profiles can then be estimated based on the values of S_p and β_p.

[11] The aerosol optical properties processing (i.e., forward inversion) proceeds downward throughout each particulate layer until $T_p(z) < T_L$ or until the signal from the Earth's surface is detected, where T_L is a lower limit defined through error consideration. Extensive automated use of this algorithm has been incorporated into both the Global Backscatter Experiment (GLOBE) with aircraft lidar and analysis of ground-based MPL data from a 1998 field experiment at the Atmospheric Radiation Measurement (ARM) program site in Oklahoma [*Hlavka et al.*, 1998].

[12] To obtain an estimate of the aerosol optical depth for a layer requires estimation of the aerosol S-ratio, S_p. S-ratios

are assigned for every layer in every profile for every wavelength. There are two ways to obtain a value for S_p. The preferred method is to use a transmission loss calculation whereby S_p is calculated directly from the lidar data. This approach is practical only for a cloud or elevated aerosol layer that is optically thin with either a lower layer or the Earth's surface sensed below it and has enough clear air (no aerosols) immediately below the layer to determine signal loss through the layer. The clear air zone must be at least a minimum thickness (around 0.6 km) and analysis is usually restricted to 3 km thickness. Ice clouds above 5 km are the most likely candidates for this analysis, although elevated aerosol layers with enough clean air below are also appropriate. Under these conditions, an estimate of $T_p(z)$, and thus an estimate of effective optical depth for the layer, can be determined.

[13] To use the transmission loss method the layer top and bottom boundaries, z_t and z_b, must first be determined and the bounds of the clear air zone, from z_b down to some altitude z_c must be defined. The two-way particulate transmission to the bottom of the layer, $T_p^2(z_b)$, can then be calculated:

$$T_p^2(z_b) = \frac{\int_{z_b}^{z_c} P(z)dz}{T_m^2(z_b)\int_{z_b}^{z_c} \beta_m(z)T_m^2(z)dz} \quad (4)$$

The boundary condition, I_B, at the top (z_t) or bottom (z_b) of any layer can be defined as:

$$I_B(z_{t,b}) = T_p^2(z_{t,b})T_m^{2\chi}(z_{t,b}) \quad (5)$$

where $\chi = S_p/S_m$ and $T_m^{2\chi} = e^{-2\chi\int \sigma_m dz}$. S_p can then be calculated through an iterative solution to the following equation:

$$S_p = \frac{I_B(z_t) - I_B(z_b)}{2\int_{z_t}^{z_b} P(z)T_m^{2(\chi-1)}(z)dz} \quad (6)$$

An initial value of S_p is used to start the iteration and computation continues until the solution converges to a set tolerance. A similar version of this analysis method has worked well during automated MPL data processing [*Welton et al.*, 2002].

[14] In practice, the transmission loss technique works best at 532 nm because there is sufficient molecular return below layers to accurately calculate the signal loss. At 1064 nm the transmission loss method is not effective because lower signal-to-noise and near absence of molecular return produce large uncertainties. Because the transmission loss calculation of S_p requires a clear air zone below the layer, direct calculation of PBL S-ratio is not possible. Even with the many caveats listed above, the transmission loss method is preferred because S_p can be estimated without assumptions of aerosol climatology.

[15] In most cases it will not be possible to calculate S_p directly from the lidar data. For atmospheric layers where S_p cannot be calculated a value must be assigned for each layer. In these cases, S_p can either be chosen based on predefined look-up matrices of S_p, distinguishing between different cloud and aerosol regimes (including differentiating between elevated and boundary layer aerosol), or S_p can be estimated from an independent instrument. When an assignment must be made, the preferred approach is to use optical depth measurements from ground-based or airborne instruments (AERONET, MPL, or AATS-14) to provide an independent measurement with which to constrain the lidar inversion. Using an independently measured optical depth allows the lidar inversion to be constrained to match that value and allows an estimate of S_p to be calculated. Because Sun photometers provide only column optical depth, the CPL profile is used to ensure that clouds and elevated aerosol layers either were not present over the Sun photometer site or, if present, that the transmission losses are taken into account. For the SAFARI campaign ground-based and airborne Sun photometer data was rather plentiful, thereby providing frequent constraint of the CPL data processing. Away from Sun photometer sites determination of S_p for aerosol (noncloud) will be driven by geographic location, layer height, and relative humidity, with geographic location the most important factor. Geographic location can be divided into three main aerosol regimes: continental, desert, and maritime [*Ackermann*, 1998; *Welton et al.*, 2000].

[16] The tropospheric and PBL S-ratio default values are primarily formulated from a method developed by *Ackermann* [1998] that relates relative humidity to S-ratio in three geographic regions: maritime, continental, and desert. As stated previously, the CPL data alone does not permit a unique retrieval of S-ratios for processing of PBL aerosol optical properties. However, other instruments, such as AERONET Sun photometers, can provide optical depth measurements that can be used to constrain the lidar inversion and thereby permit computation of S-ratios from the lidar data. Enough overflights of AERONET sites will allow compilation of a regional S-ratio assignment matrix that can be used rather than defaulting to a generic look-up table. For an experiment like SAFARI where AERONET sites were frequently overflown, a regional S-ratio matrix based on local measurements and regional climatology permits more accurate optical depth estimates than using a generic S-ratio matrix.

[17] Finally, a brief discussion of the CPL calibration method and accuracy is required. The accuracy of all derived data products is dependent upon how well the lidar can be calibrated. A common lidar calibration method is to match the measured lidar profile to a measured or calculated Rayleigh profile at high altitudes. Because the CPL flies at high altitudes it is straightforward to choose a calibration region that is free of cloud and aerosol contamination. Typically, the CPL calibration is performed in a 2-km zone within the 12–17 km altitude region in areas where no cirrus are present. The calibration region can be adjusted as necessary to avoid cloud or stratospheric aerosol contamination. In this altitude region the Rayleigh signal is strong enough to allow an accurate calibration at both 532 nm and 1064 nm.

[18] The CPL data processing algorithm attempts to calibrate every profile unless clouds are present in the

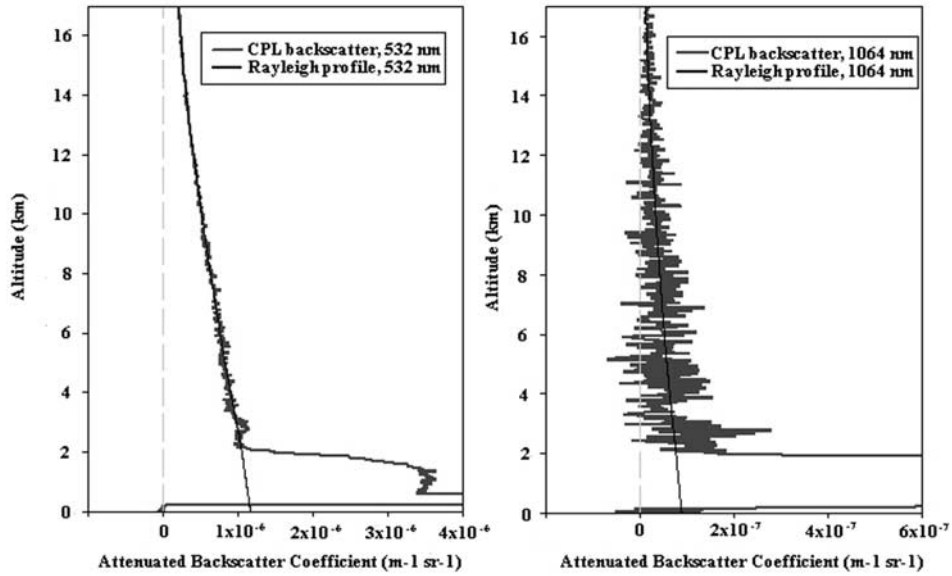

Figure 1. Examples of CPL calibration profiles at 532 nm (left) and 1064 nm (right). The smooth solid black line is the calculated Rayleigh profile to which the lidar profile is matched. In this example the calibration region was selected to be 13–15 km. The calibrated lidar profile matches the Rayleigh profile nicely down to the PBL where aerosols cause enhanced scattering.

calibration region. Calibration values from 1-s averaged profiles are further averaged to 5-min resolution, and the 5-min data is curve fit to produce a polynomial calibration equation for each wavelength. The average standard deviation of the 1-s calibration values within each 5-min average is 4.8% at 532 nm and 37.8% at 1064 nm. The uncertainty of the calibration curve fit, given as the average fit residual, over entire flights is 4.0% at 532 nm and 3.7% at 1064 nm, demonstrating that we can accurately calibrate the CPL using 5-min averages, including the noisier 1064 nm profiles. Figure 1 demonstrates the Rayleigh calibration for both 532 nm and 1064 nm. Figure 1 shows a 30-s average of CPL data overplotted on a calculated Rayleigh profile. It is seen that the CPL signal follows the Rayleigh signal down to the PBL, and the noise excursions on the signal are small.

3. PBL Optical Depth Estimates

[19] A prime reason to use the ER-2 aircraft during SAFARI was to obtain measurements in widely varying regions of southern Africa. Figure 2 shows a composite of the PBL aerosol optical depth derived from the 1064 nm CPL measurements. Figure 3 shows the corresponding composite picture derived from the 532 nm measurements. For these composite images the 1-s data were averaged into 2 min intervals. Data from 13 flights (22, 24, 25, 27, 29, 31 August and 1, 4, 6, 7, 11, 13, 14 September) are included in these images. Areas where no PBL was detected (due, e.g., to clouds above or low signal) are not plotted.

[20] From Figures 2 and 3 it is evident that different regions are generally associated with differing levels of PBL aerosol optical depth. To aid in understanding the various regions four sectors were defined, with each sector being generally associated with distinct land characteristics [*Le Canut et al.*, 1996] and different levels of industrialization and/or biomass burning. Sector 1, off the east coast and including the Lowveld region, is a nonindustrial, largely savanna region that was subject to heavy biomass burning. Sector 2 includes the heavily industrialized Highveld region. Sector 3 is also industrialized and includes Zambia, where extensive biomass burning was occurring during the SAFARI campaign. Finally, sector 4 is characterized coastal, mostly nonindustrialized, and some desert areas.

[21] The four sectors, while only grossly defined, provide a means of characterizing the aerosol properties of different regions. Table 1 presents mean values of the PBL aerosol optical depth for each sector. Also provided in Table 1 is the mean color ratio (ratio of backscatter values, β_{532}/β_{1064}) for each sector. Sector 1 is seen to have a large value of mean optical depth as well as the largest value of color ratio. Sectors 3 and 4 have smaller values of mean optical depth and smaller color ratios.

[22] To quantify the information contained in Figures 2 and 3, histograms of the PBL aerosol optical depth were generated for both 532 and 1064 nm in each sector. The histograms are displayed in Figures 4 and 5. The histograms of 532 nm aerosol optical depth (Figure 4) show markedly different structure in each sector. Not surprisingly, sector 4, off the Namibian coast, has the lowest overall optical depth and also the smallest spread in distribution. Also not unexpected is the distribution of sector 3, which displays a large spread in derived optical depth as well as the highest peak value for the aerosol optical depth.

[23] The histograms of 1064 nm aerosol optical depth (Figure 5) also exhibit different features in each sector. As with the 532 nm data, sector 3 again has the largest spread in derived values resulting from the overall increased level of pollution in that sector. Interestingly, sector 4 shows a greater relative spread in values than does the 532 nm data, and reasons for this are not completely certain. It can be speculated that sector 4 contains more airborne dust and sea

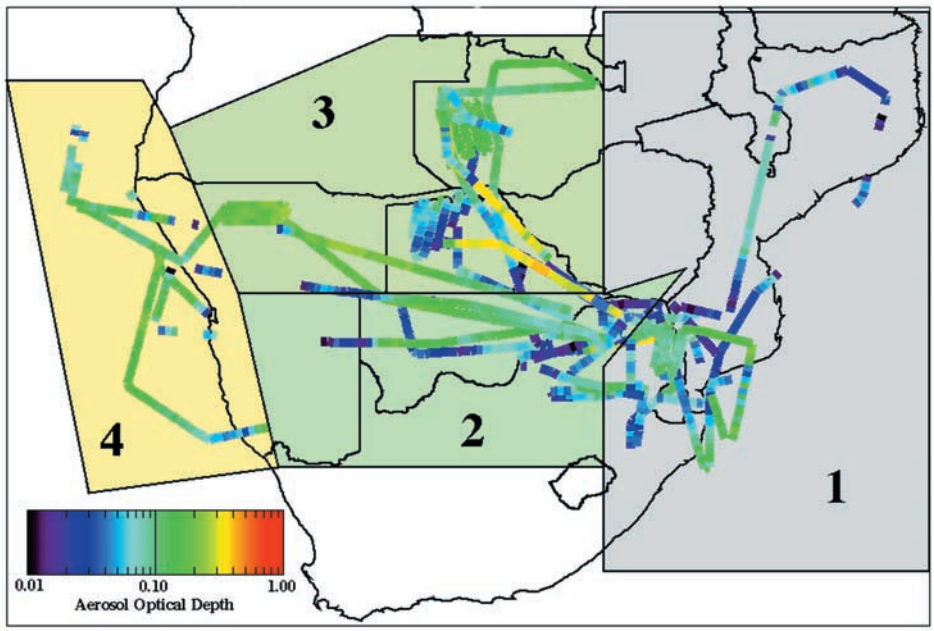

Figure 2. Composite map of CPL-derived 1064 nm PBL aerosol optical depth. Aerosol optical depth magnitude is denoted by the color scale. Four sectors have been defined based on differing geographical and industrial characteristics (see text).

salt from nearby desert and maritime regions and therefore the 1064 nm signal is affected more strongly than the 532 nm signal.

4. Aerosol Extinction Profile Estimates

[24] In addition to the PBL aerosol optical depth it is useful to examine the CPL-derived PBL aerosol extinction profiles in each sector. Rather than producing an average extinction profile from all measurements in a given sector, 10-min average profiles were generated. Aerosol extinction estimates derived from long time averages of CPL data will have large error bars owing to several factors, a primary factor being natural variability in the atmosphere. The shorter averaging period minimizes natural variability to more clearly illustrate the

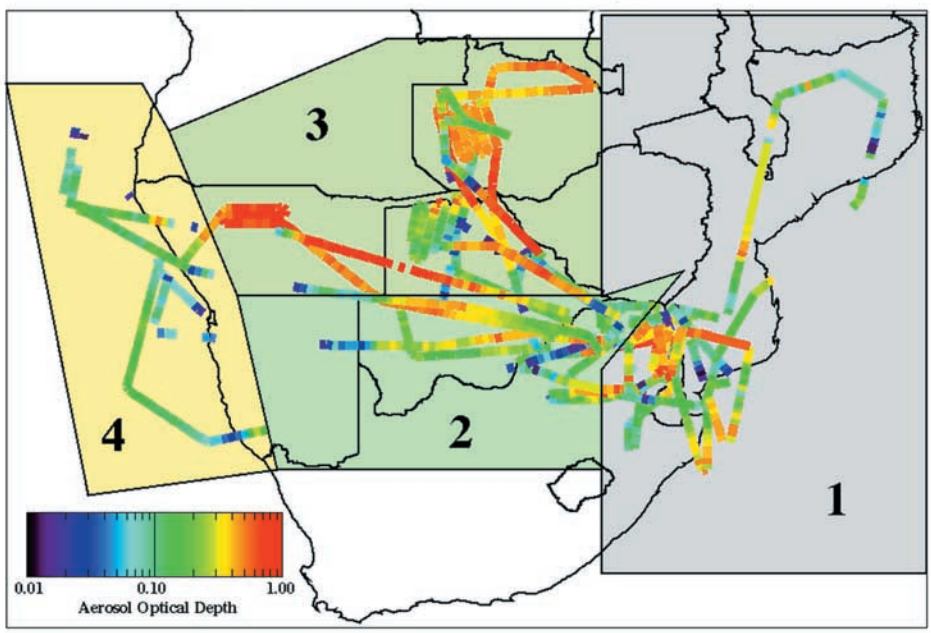

Figure 3. Same as Figure 2, but for 532 nm PBL aerosol optical depth.

Table 1. Mean Values of PBL Aerosol Optical Depth and Color Ratio by Sector

	Sector 1	Sector 2	Sector 3	Sector 4
532 nm mean optical depth	0.280 ± 0.183	0.226 ± 0.158	0.396 ± 0.216	0.148 ± 0.113
1064 nm mean optical depth	0.084 ± 0.059	0.081 ± 0.061	0.141 ± 0.099	0.134 ± 0.084
mean color ratio β532/β1064	2.051 ± 0.428	1.764 ± 0.429	1.801 ± 0.093	1.416 ± 0.212

uncertainty due to signal level and instrumental effects. Figure 6 displays the 10-min averages of PBL aerosol extinction. In all cases, only profiles with no cloud contamination were included in the averages, and lofted layers were excluded to show only the PBL extinction. Note that the altitude scale in Figure 6 is referenced to sea level, thus the extinction profiles end at the mean ground level. Standard deviations of the extinction profiles are shown as the gray-shaded areas in Figure 6. In all cases, the error bars are approximately 50%.

[25] The aerosol extinction at 532 nm in sectors 1–3 is greater than at 1064 nm at all altitudes because the aerosols are primarily products of fresh biomass burning and industrial pollution, which contain relatively small particles. In these areas of heavy biomass burning, calculated S-ratios in the PBL tend be large (>50 sr, see Table 2). As *Franke et al.* [2001] have noted, large S-ratios indicate the presence of small, highly absorbing aerosol particles. Large error bars in sector 3 near the ground are caused by attenuation of the 532 nm signal owing to heavy biomass burning.

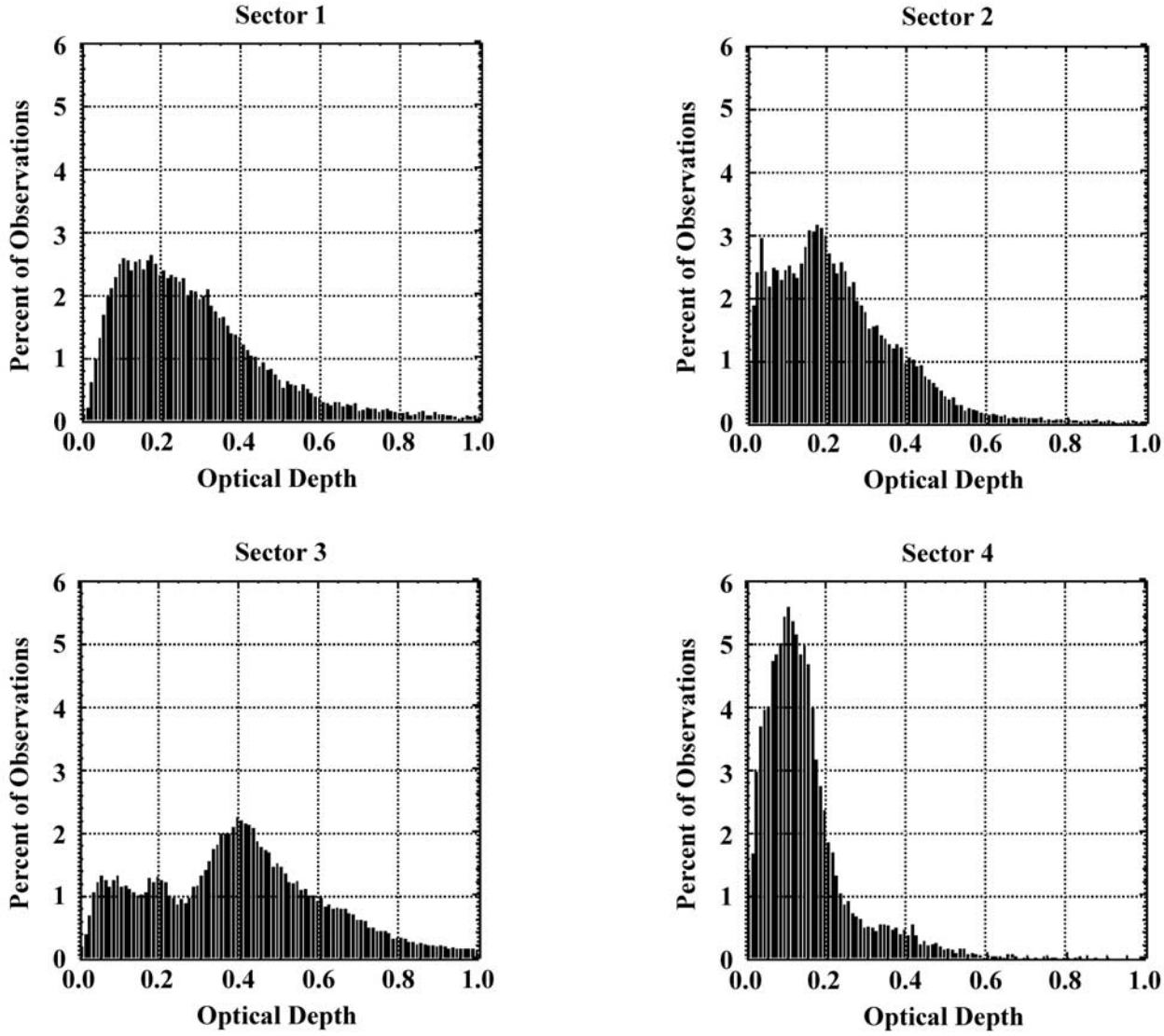

Figure 4. Histograms of 532 nm PBL aerosol optical depth by sector as a percentage of total observations. Sector numbers correspond to those defined in Figures 2 and 3. Optical depth measurements are binned in 0.01 increments.

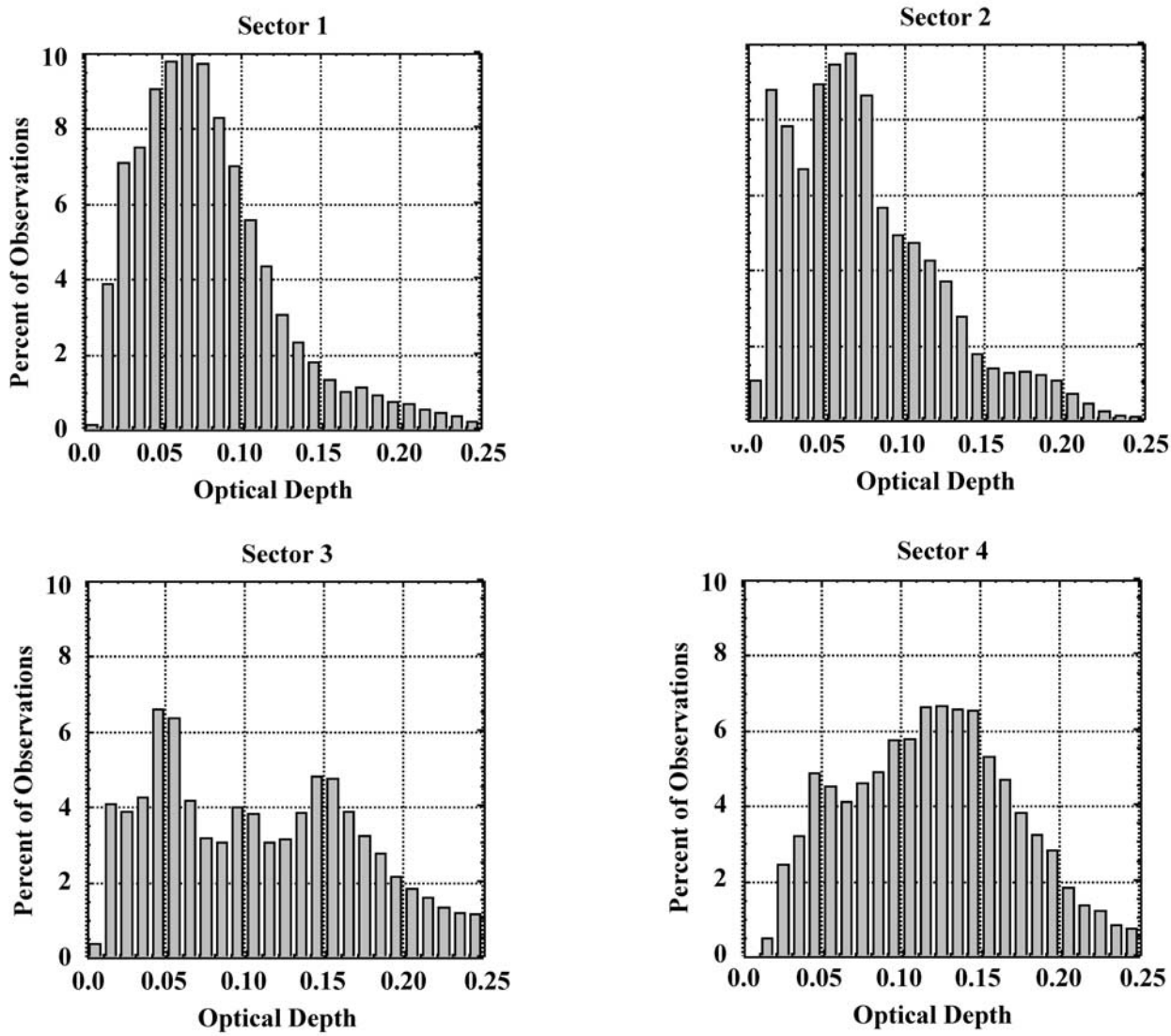

Figure 5. Same as Figure 4, except for 1064 nm PBL aerosol optical depth.

[26] Sectors 1 and 3 show the greatest uncertainties due to the predominance of biomass burning occurring in those regions, which results in increased signal attenuation and greater variability in the vicinity of fire sources. The PBL top in sectors 1–3 is quite high, as confirmed by meteorological soundings. The flights generally took place in mid- to late-morning, which is the time when nocturnal inversions break down and the top of the PBL rises. Sector 4 shows a typical shallow and tightly capped marine boundary layer off the coast of Namibia. In the marine PBL the extinction coefficients for both 532 and 1064 nm are roughly the same, which is characteristic of the relatively large aerosol particles that exist in marine boundary layers.

[27] Continuous time-height profiles of aerosol extinction can be derived from CPL data. Figure 7 shows an example from 24 August 2000 off the east coast of South Africa and over Inhaca Island. Note the elevated aerosol layer propagating from the Highveld region out over the Indian Ocean, and the distinct clear band between the elevated aerosol and the marine boundary layer. We note that of the many instruments involved in SAFARI, only the two lidar instruments (airborne CPL and ground-based MPL) have the capability to provide continuous range-resolved profiles of aerosol backscatter and extinction estimates.

[28] The CPL data can also be used to calculate the S-ratio in regions where there are elevated aerosol layers, as frequently occurs off the coast of Namibia [*Carlson and Prospero*, 1972]. Under such conditions direct retrievals of the S-ratio of elevated aerosol layers were occasionally calculated using the transmission-loss method described earlier. A good example is a prolonged interval of the 14 September flight near the coast of Namibia. Figure 8 shows an image of the extinction retrievals plus a plot of the calculated S-ratio in the elevated aerosol layer. The elevated layer was transported from the continent out over the ocean and is undoubtedly a mixture of smoke and dust. Presence of smoke in the elevated layer is not unexpected since the heaviest biomass burning was occurring in and to the north of Zambia (within sector 3). This agrees with the study by

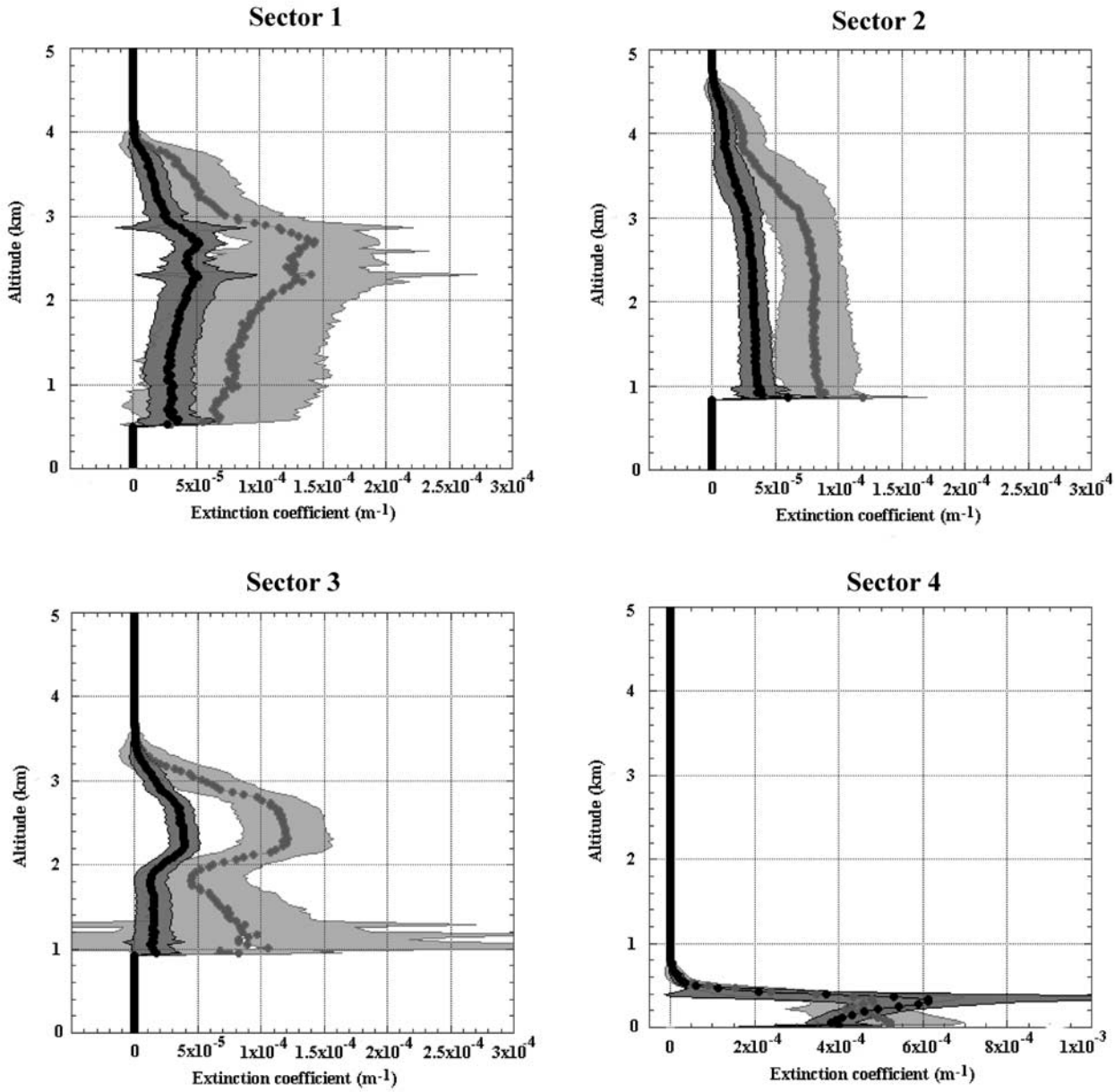

Figure 6. Profiles of PBL aerosol extinction by sector. Profiles are 10-min averages. Sector numbers correspond to those defined in Figures 2 and 3. In each panel the black line is 1064 nm extinction and the gray line is 532 nm extinction. Shaded regions define the standard deviations. Only profiles with no cloud contamination are included in the averages, and any lofted aerosol layers are not included. Altitude is above sea level, thus sectors 1, 2 and 3 end at the mean ground elevation. (Note that the sector 4 graph has a different *x* axis scale.)

Cahoon et al. [1992], who clearly shows the predominance of burning during the August–September period occurs, generally, north of 25 degrees south latitude. A fit to the S-ratios shows the values rising with time, starting near 40 sr and increasing toward 60 sr. S-ratio values between 40–60 sr are in good agreement with those tabulated by *Ackerman* [1998] and *Voss et al.* [2001] for smoke particles. Data is only available for the 532 nm channel due to the inherently

Table 2. CPL PBL S-Ratio Tendencies as a Function of Aerosol Loading[a]

Aerosol Category	Average S-ratio 532 nm	Average S-ratio 1064 nm	Number of Observations
light aerosol (532 nm O.D.< 0.3)	42.5 ± 7.6 sr	31.9 ± 4.7 sr	7
moderate aerosol (532 nm O.D. 0.3–0.5)	53.0 ± 4.9 sr	33.7 ± 2.7 sr	8
heavy aerosol (532 nm O.D. 0.5–1.0)	72.2 ± 2.0 sr	35.4 ± 6.0 sr	8

[a]S-ratios are 30-s averages calculated by tying the lidar inversion to Aeronet Sun photometer measurements during direct overflights.

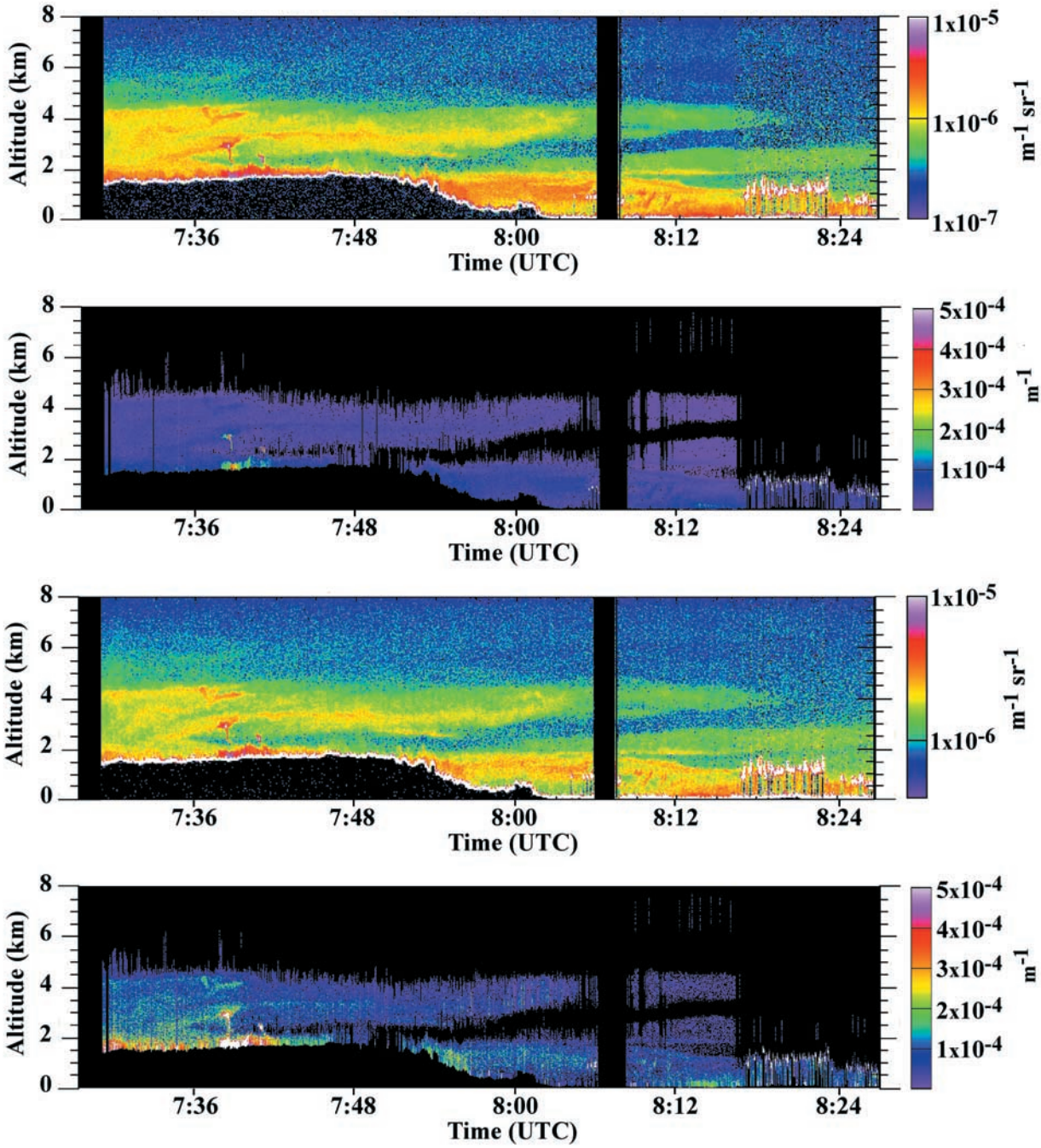

Figure 7. CPL data segment from 24 August 2000 showing elevated aerosol layer above west coast over Inhaca Island. (a) 1064 nm attenuated backscatter profiles; (b) 1064 nm aerosol extinction profiles; (c) 532 nm attenuated backscatter profiles; and (d) 532 nm aerosol extinction profiles.

weak 1064 nm backscatter in the clean air below the layer. In these particular examples the 1064 nm molecular return is too weak to calculate signal loss through the layer, as is typically the case at 1064 nm.

[29] Whenever the ER-2 aircraft overflew an AERONET Sun photometer site the CPL analysis could calculate an S-ratio for the PBL layer using the AERONET optical depth measurement as a constraint on the lidar inversion. Tabulation of results from overflights of AERONET sites across southern Africa allowed categorizations of the CPL-derived aerosol S-ratio as a function of derived aerosol optical depth, as shown in Table 2. The largest component of the aerosol loading was smoke particles, although dust and other pollutants also contribute. Smoke particles are relatively small and this property is characterized by a large wavelength dependence on the S-ratio as the smoke loading becomes dominant. The 532 nm channel is attenuated much more quickly in smoke-filled PBLs compared to the 1064

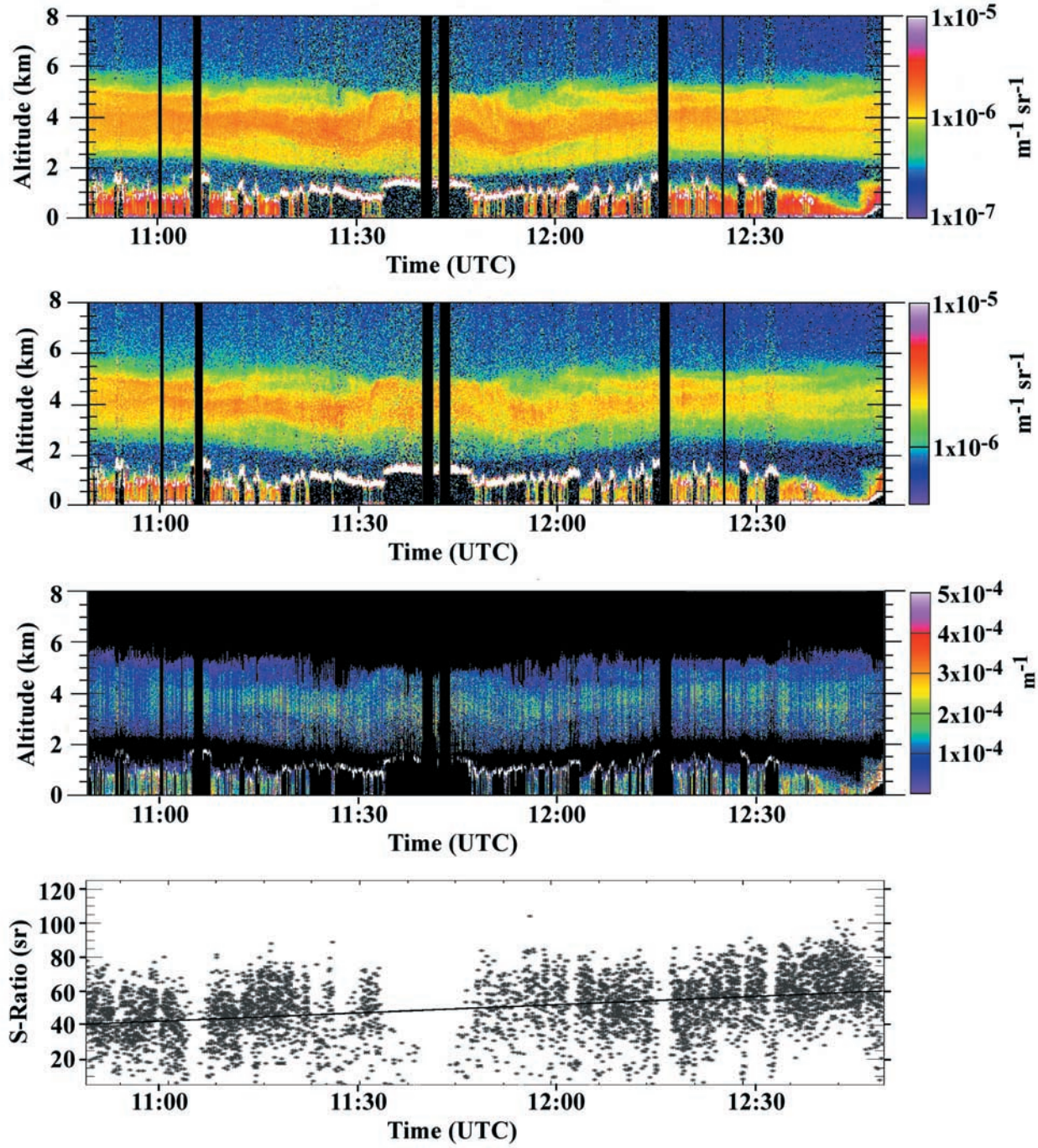

Figure 8. Two-hour data segment from 14 September 2000 showing elevated aerosol layer off the west coast of Namibia. (a) 1064 nm attenuated backscatter profiles; (b) 532 nm attenuated backscatter profiles; (c) 532 nm aerosol extinction profiles; and (d) S-ratio of elevated aerosol layer derived from 532 nm data using the transmission loss method.

nm channel. Based on the results in Table 2 we can conclude that smoke has only a small effect on the S-ratio at 1064 nm.

5. Comparisons With Other Instruments

[30] At several times during the campaign the ER-2 was directed to overfly the MPL sites to allow calibration and comparison of the ground-based and airborne sensors. Figure 9 shows a comparison of extinction profiles derived from the CPL and MPL on 29 August 2000 over Skukuza. The CPL profile is a 30-s average while the MPL profile is a 30-min average. In calculating the extinction profiles the S-ratio for the CPL 532 nm channel was calculated to be 46.5 sr while the MPL (operating at 523 nm) S-ratio calculations ranged from 49 to 85 sr for the three profiles shown in

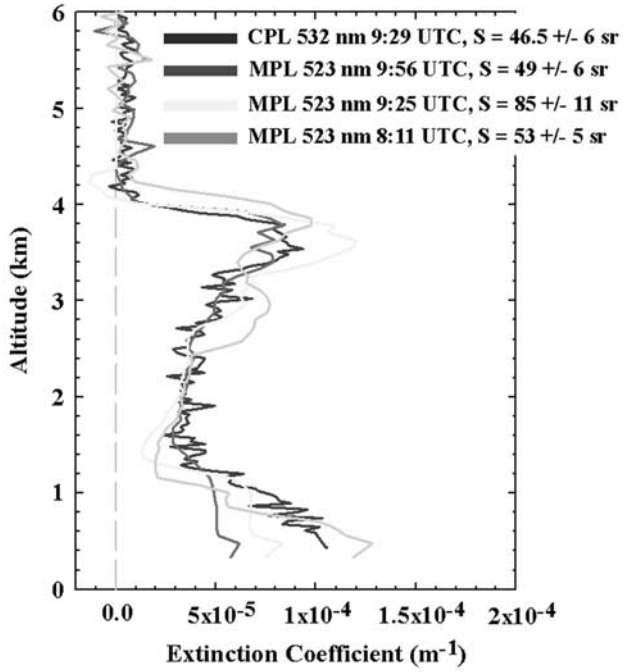

Figure 9. Comparison of extinction profiles from CPL (black profile) and MPL (3 gray profiles) on 29 August 2000 at Skukuza. CPL profile is a 30-s average. MPL profiles are 30-min averages centered at the times listed. Differences in the lowest km are due to aerosol inhomogeneity during the measurements. Altitude is above sea level.

Figure 9. Both lidars used AERONET optical depth measurements [*Holben, et al.*, 1998] colocated near the MPL site to calculate the S-ratios. The PBL aerosol optical depth was estimated to be 0.21.

[31] Agreement between the two lidars is excellent at altitudes above ~1 km. In the lowest km there is some divergence in the measurements. Close examination revealed that the divergence is due to sampling of different volumes in a PBL that was far from homogeneous and is not due to instrument effects such as near-field overlap of the MPL. Also contributing to discrepancies at the lowest altitudes is the fact that the CPL profile is an average along ~6 km compared to the stationary MPL measurements. For this reason, MPL profiles are shown from one hour prior to the overflight, during the overflight, and one hour after the overflight. As can be seen, considerable variability occurs in the lowest km. The degree of variability is not unexpected, as the measurements were made in the morning hours when extensive biomass burning was occurring near the MPL site. MPL data taken during the morning periods routinely shows plumes of intense aerosol loading at the lowest levels as grass fires were set in the immediate vicinity of the MPL site.

[32] Figure 10 shows a single CPL-MPL comparison at the Mongu site on 1 September 2000. For this example the S-ratio for the CPL was calculated to be 55.7 sr and the MPL S-ratio was calculated to be 88.1 sr. The optical depth was determined to be 0.70 during this intercomparison period. The agreement in this comparison is not as good as at Skukuza, and there are several reasons for the discrepancy. First, the overflight time was after sunset, so the AERONET optical depth has to be extrapolated from measurements made before sunset. Second, the same caveat applies as in Figure 8, namely that the CPL is a 30-s average along the ER-2 flight track whereas the MPL is a 30-min average at a stationary location. And third, there is a slight wavelength difference between the CPL and MPL.

[33] The primary point of interest between the Skukuza and Mongu comparisons, however, is to illustrate the large difference in the derived PBL extinction profiles between the two sites. The extinction coefficients at the Mongu site are a factor 2–4 greater than at the Skukuza site. Again, this is not surprising given the predominance of biomass burning at the lower-latitude Mongu site compared to Skukuza at that time of year [*Cahoon et al.*, 1992]. Also, note that the degree of vertical variability is greater for the Skukuza case than for Mongu. CPL measurements repeatedly revealed complex PBL vertical structure over Skukuza and the Lowveld region, whereas PBL structure in more northerly regions was more vertically homogeneous.

[34] The Ames Airborne Tracking 14-channel Sun photometer (AATS-14) onboard the University of Washington CV-580 aircraft was also used extensively to validate CPL and MPL measurements. The AATS-14 measures atmospheric transmission (and hence optical depth and extinction) in bands from 354 nm out to 1558 nm [*Schmid et al.*, 2000]. The channels of interest to CPL are those at 525 nm and 1020 nm, close to the CPL wavelengths. In all cases there was good agreement between CPL and the AATS-14, although in many cases comparisons in the lowest km suffered from variability due to inhomogeneity and different sampling volumes. Comparisons between CPL and AATS-14 are treated extensively in a companion paper by *Schmid et al.* [2003]. One of the CPL-AATS comparisons

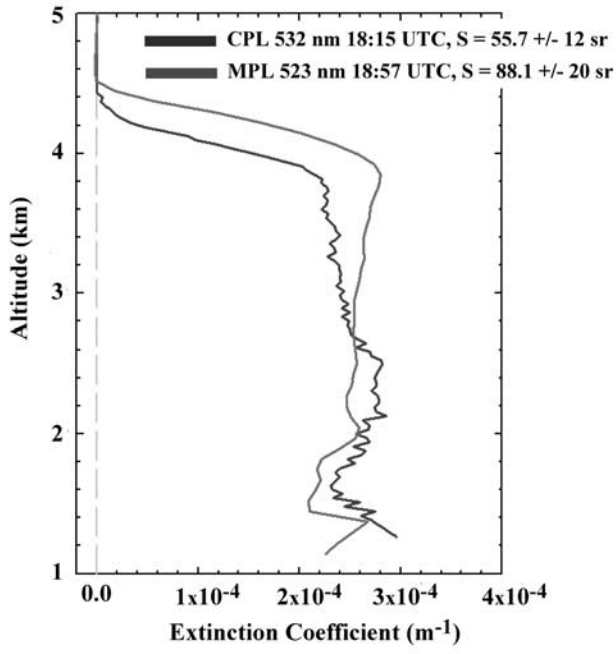

Figure 10. Comparison of extinction profiles from CPL (black profile) and MPL (gray profile) on 1 September 2000 at Mongu, Zambia. Note difference in magnitude and vertical structure compared to Figure 9. Altitude is above sea level.

[*Schmid et al.*, 2003, Figure 9] is taken over Inhaca Island on 24 August, corresponding to time 0810 UTC in Figure 7.

6. Conclusion

[35] The SAFARI field campaign during August–September 2000 provided an opportunity to study the climatology of southern Africa. Remote sensing instruments onboard the NASA ER-2 high-altitude aircraft permitted measurements in widely varying regions with multiple sensors. The CPL was a new and unique instrument for the SAFARI campaign and provided high resolution profiles of cloud and aerosol structure. In particular, the CPL provided information on PBL optical properties and variability. As shown, the CPL can be used for wide-scale mapping of aerosol loading and these measurements will prove useful in aerosol transport studies. Among the instruments participating in SAFARI, the CPL was the only airborne instrument capable of providing continuous, range-resolved profiles of aerosol extinction estimates revealing detailed vertical structure that was not available from other instruments.

[36] Segregating the CPL measurements into sectors based on geography and degree of industrialization allows examination of aerosol properties by region. The estimates of PBL aerosol optical depth and aerosol extinction show the heaviest aerosol loading over the northern region (sectors 1 and 3). Although the sectors used here were only grossly defined it is still possible to see different features in the different regions. Future work will focus on refining the sector definitions based on better knowledge of geographical and local emission considerations.

[37] When elevated aerosol layers are present it is possible to directly estimate the S-ratio from CPL data. A case study using an elevated layer off the west coast of Namibia resulted in S-ratios between 40–60 sr at 532 nm, which is consistent with S-ratios expected for smoke. In nonelevated layers (e.g., PBL) it is not possible to uniquely calculate S-ratios from lidar data. However, optical depth measurements from AERONET or AATS-14 Sun photometers can be used to constrain the lidar inversion. In such cases, PBL S-ratios were calculated to be 42–72 sr at 532 nm and 32–35 sr at 1064 nm.

[38] Comparison of aerosol extinction profiles derived from CPL with those derived from ground-based MPL systems show good agreement. There is, however, some discrepancy in the lowest km. Detailed investigation revealed that the discrepancy is caused by aerosol inhomogeneity in the lowest levels of the PBL. Comparisons with the AATS-14 Sun photometer, shown in a companion paper, also show good agreement.

[39] **Acknowledgments.** The Cloud Physics Lidar is sponsored by NASA's Earth Observing System (EOS) office and by NASA Radiation Sciences, Code YS. We also thank Beat Schmid of the Bay Area Environmental Research Institute for his efforts in comparing CPL and AATS-14 data, and Brent Holben of AERONET for access to Cimel Sun photometer data. Data presented was collected as part of the Southern African Regional Science Initiative (SAFARI-2000) field campaign.

References

Ackermann, J., The extinction-to-backscatter ratio of tropospheric aerosol: A numerical study, *J. Atmos. Oceanic Technol.*, *15*, 1043–1050, 1998.

Cahoon, D. R., Jr., B. J. Stocks, J. S. Levine, W. R. Cofer, and K. P. O'Neill, Seasonal distribution of African savanna fires, *Nature*, *359*, 812–815, 1992.

Campbell, J., E. J. Welton, J. D. Spinhirne, Q. Ji, S.-C. Tsay, S. J. Piketh, M. Barenbrug, and B. N. Holben, Micropulse lidar observations of tropospheric aerosols over northeastern South Africa during the ARREX and SAFARI-2000 dry season experiments, *J. Geophys. Res.*, *108*, doi:10.1029/2002JD002563, in press, 2003.

Carlson, T. N., and J. M. Prospero, The long-range movement of Saharan air outbreaks over the northern equatorial Atlantic, *J. Appl. Meteorol.*, *11*, 283–297, 1972.

Franke, K., A. Ansmann, D. Muller, D. Althausen, F. Wagner, and R. Scheele, One-year observations of particle lidar ratio over the tropical Indian Ocean with Raman lidar, *Geophys. Res. Lett.*, *28*, 4559–4562, 2001.

Hlavka, D. L., J. D. Spinhirne, and J. R. Campbell, Aerosol analysis techniques and results from micro pulse lidar, in *Proceedings of 19th International Laser Radar Conference, Annapolis, MD, July 6–10*, Natl. Tech. Inf. Serv., Springfield, Va., 1998.

Holben, B. N., et al., AERONET—A federated instrument network and data archive for aerosol characterization, *Remote Sens. Environ.*, *66*, 1–16, 1998.

Hutt, D. L., L. R. Bissonnette, and L. Durand, Multiple field of view lidar returns from atmospheric aerosols, *Appl. Opt.*, *33*, 2338–2347, 1994.

King, M. D., et al., Remote sensing of smoke, land, and clouds from the NASA ER-2 during SAFARI-2000, *J . Geophys. Res.*, *108*, doi:10.1029/2002JD002307, in press, 2003.

Le Canut, P., M. O. Andreae, G. W. Harris, F. G. Wienhold, and T. Zenker, Airborne studies of emissions from savanna fires in southern Africa, 1, Aerosol emissions measured with a laser optical particle counter, *J. Geophys. Res.*, *101*, 23,615–23,630, 1996.

McGill, M. J., D. L. Hlavka, W. D. Hart, V. S. Scott, J. D. Spinhirne, and B. Schmid, The Cloud Physics Lidar: Instrument description and initial measurement results, *Appl. Opt.*, *41*, 3725–3734, 2002.

Schmid, B., et al., Clear-sky studies of lower tropospheric aerosol and water vapor during ACE-2 using airborne sunphotometer, airborne in-situ, space-borne, and ground-based measurements, *Tellus, Ser. B*, *52*, 568–593, 2000.

Schmid, B., et al., Coordinated airborne, spaceborne, and ground-based measurements of massive, thick aerosol layers during the dry season in Southern Africa, *J. Geophys. Res.*, *108*, doi:10.1029/2002JD002297, in press, 2003.

Spinhirne, J. D., J. A. Reagan, and B. M. Herman, Vertical distribution of aerosol extinction cross section and inference of aerosol imaginary index in the troposphere by lidar technique, *J. Appl. Meteorol.*, *19*, 426–438, 1980.

Swap, B., J. Privette, M. King, D. Starr, T. Suttles, H. Annegarn, M. Scholes, and C. O. Justice, SAFARI 2000: A southern African regional science initiative, *Eos Earth Obs.*, *10*(6), 25–28, 1998.

Swap, R. J., H. J. Annegarn, and L. Otter, Southern African Regional Science Initiative (SAFARI 2000): Summary of science plan, *S. Afr. J. Sci.*, *98*, 119–124, 2002.

Swap, R. J., et al., The Southern African Regional Science Initiative (SAFARI 2000): Overview of the dry season field campaign, *S. Afr. J. Sci.*, *98*, 125–130, 2002.

Voss, K. J., E. J. Welton, P. K. Quinn, J. Johnson, A. Thompson, and H. Gordon, Lidar measurements during Aerosols99, *J. Geophys. Res.*, *106*, 20,821–20,832, 2001.

Welton, E. J., et al., Ground-based lidar measurements of aerosols during ACE-2: Instrument description, results, and comparisons with other ground-based and airborne measurements, *Tellus, Ser. B*, *52*, 635–650, 2000.

Welton, E. J., J. R. Campbell, J. D. Spinhirne, V. S. Scott, Global monitoring of clouds and aerosols using a network of micro-pulse lidar systems, in *Lidar Remote Sensing for Industry and Environmental Monitoring*, *Proc. SPIE*, edited by U. N. Singh, T. Itabe, and N. Sugimoto, pp. 151–158, Int. Soc. for Opt. Eng., Bellingham, Wash., 2001.

Welton, E. J., K. J. Voss, P. K. Quinn, P. J. Flatau, K. Markowicz, J. R. Campbell, J. D. Spinhirne, H. R. Gordon, and J. E. Johnson, Measurements of aerosol vertical profiles and optical properties during INDOEX 1999 using micro-pulse lidars, *J. Geophys. Res.*, *107*(19), 8019, doi:10.1029/2002JD000038, 2002.

J. R. Campbell, W. D. Hart, and D. L. Hlavka, Science Systems and Applications, Inc., NASA Goddard Space Flight Center, Code 912, Greenbelt, MD 20771, USA. (campbell@virl.gsfc.nasa.gov; billhart@virl.gsfc.nasa.gov; sgdlh@virl.gsfc.nasa.gov)

M. J. McGill, NASA Goddard Space Flight Center, Code 912, Greenbelt, MD 20771, USA. (mcgill@virl.gsfc.nasa.gov)

E. J. Welton, Goddard Earth Sciences and Technology Center, NASA Goddard Space Flight Center, Code 912, Greenbelt, MD 20771, USA. (welton@virl.gsfc.nasa.gov)